Inorg. Chem. **2009**, *48*, 128−137

Single-Ion Anisotropy and Exchange Interactions in the Cyano-Bridged Trimers $Mn^{III}_2M^{III}(CN)_6$ (M^{III} = Co, Cr, Fe) Species Incorporating $[Mn(5\text{-Brsalen})]^+$ Units: An Inelastic Neutron Scattering and Magnetic Susceptibility Study

Philip L. W. Tregenna-Piggott,*,† Denis Sheptyakov,† Lukas Keller,† Sophia I. Klokishner,*,‡ Sergei M. Ostrovsky,‡ Andrei V. Palii,‡ Oleg S. Reu,‡ Jesper Bendix,*,§ Theis Brock-Nannestad,§ Kasper Pedersen,§ Høgni Weihe,§ and Hannu Mutka||

Laboratory for Neutron Scattering, ETH Zürich and Paul Scherrer Institut, CH-5232 Villigen PSI, Switzerland, Institute of Applied Physics of the Academy of Sciences of Moldova, Academy str.5, Kishinev MD-2028, Moldova, Department of Chemistry, University of Copenhagen, Universitetsparken 5, DK-2100 Copenhagen, Denmark, and Institut Laue-Langevin, 6 Rue Jules Horowitz, BP 156-38042, Grenoble Cedex 9, France

Received September 8, 2008

The electronic structures of the compounds $K[(5\text{-Brsalen})_2(H_2O)_2\text{-}Mn_2M^{III}(CN)_6]\cdot 2H_2O$ (M^{III} = Co^{III}, Cr^{III}, Fe^{III}) have been determined by inelastic neutron scattering (INS) and magnetic susceptibility studies, revealing the manganese(III) single-ion anisotropy and exchange interactions that define the low-lying states of the Mn−M^{III}−Mn trimeric units. Despite the presence of an antiferromagnetic intertrimer interaction, the experimental evidence supports the classification of both the Cr(III) and Fe(III) compounds as single-molecule magnets. The value of 17(2) cm^{-1} established from AC susceptibility measurements for a spin-reversal barrier of $K[(5\text{-Brsalen})_2(H_2O)_2\text{-}Mn_2Cr(CN)_6]\cdot 2H_2O$ may be readily rationalized in terms of the energy level diagram determined directly by INS. AC susceptibility measurements on samples of $K[(5\text{-Brsalen})_2(H_2O)_2\text{-}Mn_2Fe(CN)_6]\cdot 2H_2O$ are contrary to those previously reported, exhibiting but the onset of peaks below temperatures of 1.8 K at oscillating frequencies in the range of 100−800 Hz. INS measurements reveal an anisotropic ferromagnetic manganese(III)−iron(III) exchange interaction, in accordance with theoretical expectations based on the unquenched orbital angular momentum of the $[Fe(CN)_6]^{3-}$ anion, giving rise to an $M_s \sim \pm 9/2$ ground state, isolated by ∼11.5 cm^{-1} from the higher-lying levels. The reported INS and magnetic data should now serve as a benchmark against which theoretical models that aim to inter-relate the electronic and molecular structure of molecular magnets should be tested.

1. Introduction

Since the discovery of the celebrated single-molecule magnet (SMM), Mn_{12}, and associated clusters,[1] strategies for the synthesis of SMMs have diversified to include families of compounds based on a host of other transition metal[2] and lanthanide metal[3] centers. These efforts have been coordinated with those of spectroscopists[4,5] and theoreticians[6−9] who aim to identify the magneto-structural correlations that govern the single-molecule magnet properties. The emergence of the cyanometallates as the new deliciae of the molecular magnetism community[10] has occurred from both synthetic and theoretical considerations. Hexacyanometallates of iron(III) and manganese(III) constitute excellent building blocks for the conception of molecular magnets, affording discrete clusters, one-dimensional chains, and extended networks.[11−22] The strong ligand field, inherent to the metal(III)−cyanide interaction, imposes orbital triplet ground terms for these anions, which in a high-symmetry environment results in residual orbital angular momentum and associated anisotropic exchange interactions.[8,23,24] The pres-

* Authors to whom correspondence should be addressed. E-mail: philip.tregenna@psi.ch (P.L.W.T.-P.), klokishner@yahoo.com (S.K.), bendix@kiku.dk (J.B.).
† ETH Zürich and Paul Scherrer Institut.
‡ Academy of Sciences of Moldova.
§ University of Copenhagen.
|| Institut Laue-Langevin.

10.1021/ic801727p CCC: $40.75
Published on Web 11/21/2008

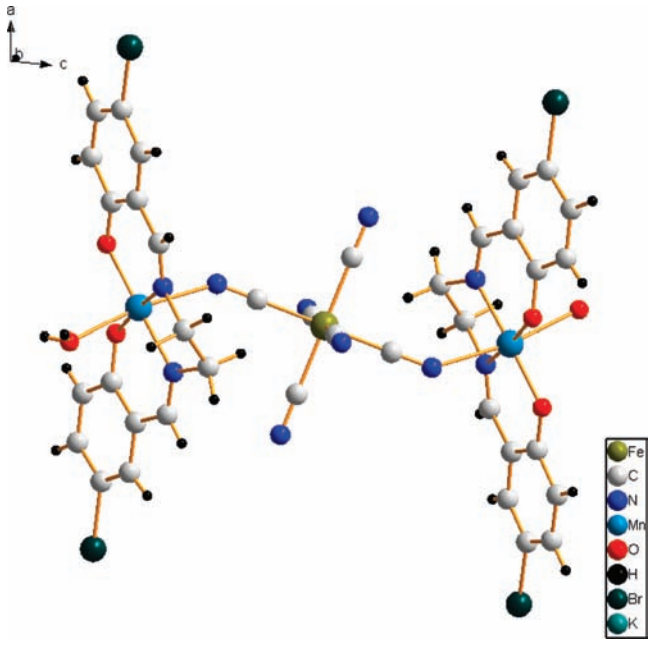

Figure 1. Structure of the MnFeMn unit, generated from ref 25.

ence of the $[Fe(CN)_6]^{3-}$ anion, in particular, is cited as a key ingredient to elevating the blocking temperature of SMMs.[8] One such example is the linear trimer, $K[(5\text{-}Brsalen)_2(H_2O)_2\text{-}Mn_2Fe(CN)_6]\cdot 2H_2O$,[12] abbreviated here to MnFeMn, consisting of the ferrous hexacyanide anion sandwiched between a pair of $[Mn(5\text{-}Brsalen)(H_2O)]$ complexes, as shown in Figure 1. MnFeMn and the chromium(III) analogue (MnCrMn) have been hailed as SMMs with spin-reversal barriers of $\sim$25 cm^{-1} and $\sim$16 cm^{-1}, respectively, on the basis of the interpretation of AC susceptibility data.[25] However, the magnitude of the out-of-phase susceptibility signal is just a fraction of that reported for other single molecular magnets—including the closely related trimer $(NEt_4)[Mn_2(salmen)_2(MeOH)_2Fe(CN)_6]$—and doubts have been raised about the reproducibility of the data.[16] Attempts to model the χ_mT data were confined to temperatures above $\sim$50 K,[25] below which the value of χ_mT falls precipitously for both MnFeMn and MnCrMn, an observation that was casually ascribed to ground-state zero-field-splittings.[25] In a more thorough analysis of the magnetic properties of MnFeMn, conducted when the compound was first reported several years earlier,[12] antiferromagnetic intertrimer interactions were introduced to model the low-temperature data. If the molecular field calculation is followed to its logical conclusion, then magnetic order is predicted to occur at $\sim$8 K for the spin-Hamiltonian parameters put forward. Whenever there is a suggestion of the onset of magnetic order, caution must be applied when interpreting AC susceptibility data, as an out-of-phase signal may not reflect the magnetic properties of the constituent

(1) Sessoli, R.; Gatteschi, D. *Angew. Chem., Int. Ed.* **2003**, *42*, 268. (a) Sessoli, R.; Tsai, H.-L.; Schake, A. R.; Wang, S.; Vincent, J. B.; Folting, K.; Gatteschi, D.; Christou, G.; Hendrickson, D. N. *J. Am. Chem. Soc.* **1993**, *115*, 1804. (b) Sessoli, R.; Gatteschi, D.; Caneschi, A.; Novak, M. A. *Nature* **1993**, *365*, 141. (c) Thomas, L.; Lionti, F.; Ballou, R.; Gatteschi, D.; Sessoli, R.; Barbara, B. *Nature* **1996**, *383*, 145. (d) Friedman, J. R.; Sarachik, M. P. *Phys. Rev. Lett.* **1996**, *76*, 3830. (e) Eppley, H. J.; Tsai, H.-L.; de Vries, N.; Folting, K.; Christou, G.; Hendrickson, D. N. *J. Am. Chem. Soc.* **1995**, *117*, 301. (f) Aubin, S. M. J.; Spagna, S.; Eppley, H. J.; Sager, R. E.; Christou, G.; Hendrickson, D. N. *Chem. Commun.* **1998**, *803*. (g) Aubin, S. M. J.; Sun, Z.; Pardi, L.; Krzystek, J.; Folting, K.; Brunel, L.-C.; Rheingold, A. L.; Christou, G.; Hendrickson, D. N. *Inorg. Chem.* **1999**, *38*, 5329. (h) Soler, M.; Chandra, S. K.; Ruiz, D.; Davidson, E. R.; Hendrickson, D. N.; Christou, G. *Chem. Commun.* **2000**, 2417. (i) Boskovic, C.; Pink, M.; Huffman, J. C.; Hendrickson, D. N.; Christou, G. *J. Am. Chem. Soc.* **2001**, *123*, 9914.

(2) Aubin, S. M. J.; Wemple, M. W.; Adams, D. M.; Tsai, H.-L.; Christou, G; Hendrickson, D. N. *J. Am. Chem. Soc.* **1996**, *118*, 7746. (a) Aubin, S. M. J.; Dilley, N. R.; Pardi, L.; Krzystek, J.; Wemple, M. W.; Brunel, L. C.; Maple, M. B.; Christou, G.; Hendrickson, D. N. *J. Am. Chem. Soc.* **1998**, *120*, 4991. (b) Andres, H.; Basler, R.; Güdel, H.-U.; Aromi, G.; Christou, G.; Buttner, H.; Ruffle, B. *J. Am. Chem. Soc.* **2000**, *122*, 12469. (c) Castro, S. L.; Sun, Z.; Grant, C. M.; Bollinger, J. C.; Hendrickson, D. N.; Christou, G. *J. Am. Chem. Soc.* **1998**, *120*, 2997. (d) Sangregorio, C.; Ohm, T.; Paulsen, C.; Sessoli, R.; Gatteschi, D. *Phys. Rev. Lett.* **1997**, *78*, 4645. (e) Schelter, E. J.; Prosvirin, A. V.; Dunbar, K. R. *J. Am. Chem. Soc.* **2004**, *126*, 15004.

(3) Ishikawa, N.; Sugita, M.; Ishikawa, T.; Koshihara, S.; Kaisu, Y. *J. Am. Chem. Soc.* **2003**, *125*, 8694. (a) Ishikawa, N.; Sugita, M.; Wernsdorfer, W. *Angew. Chem., Int. Ed.* **2005**, *44*, 2931. (b) Ishikawa, N.; Sugita, M.; Ishikawa, T.; Koshihara, S.; Kaisu, Y. *J. Phys. Chem. B.* **2004**, *108*, 11265. (c) Ishikawa, N.; Sugita, M.; Wernsdorfer, W. *J. Am. Chem. Soc.* **2005**, *127*, 3650. (d) Kido, T.; Nagasato, S.; Sunatsuki, Y.; Matsumoto, N. *Chem. Commun.* **2000**, *2113*. (e) Kido, T.; Ikuta, Y.; Sunatsuki, Y.; Ogawa, Y.; Matsumoto, N.; Re, N. *Inorg. Chem.* **2003**, *42*, 398. (f) Osa, S.; Kido, T.; Matsumoto, N.; Re, N.; Pochada, A.; Mrozinski, J. *J. Am. Chem. Soc.* **2004**, *126*, 42.

(4) Datta, S.; Waldmann, O.; Kent, A. D.; Milway, V. A.; Thompson, L. K.; Hill, S. *Phys. Rev. B: Condens. Matter Mater. Phys.* **2007**, *76*, 052407. (a) Waldmann, O.; Bircher, R.; Carver, G.; Sieber, A.; Güdel, H.-U.; Mutka, H. *Phys. Rev. B: Condens. Matter Mater. Phys.* **2007**, *75*, 174438. (b) Waldmann, O.; Carver, G.; Dobe, C.; Sieber, A.; Güdel, H.-U.; Mutka, H. *J. Am. Chem. Soc.* **2007**, *129*, 1526. (c) Sieber, A.; Foguet-Albiol, D.; Waldmann, O.; Ochsenbein, S. T.; Carver, G.; Mutka, H.; Fernandez-Alonso, F.; Mezouar, M.; Weber, H. P.; Christou, G.; Güdel, H.-U. *Phys. Rev. B: Condens. Matter Mater. Phys.* **2006**, *74*, 024405.

(5) Accorsi, S.; Barra, A. L.; Caneschi, A.; Chastanet, G.; Cornia, A.; Fabretti, A. C.; Gatteschi, D.; Mortalo, C.; Olvieri, E.; Parenti, F.; Sessoli, R.; Sorace, L.; Wernsdorfer, W.; Zobbi, L. *J. Am. Chem. Soc.* **2006**, *128*, 4742–4755. (a) Barra, A. L.; Caneschi, A.; Cornia, A.; Gatteschi, D.; Gorini, L.; Heiniger, L. P.; Sessoli, R.; Sorace, L. *J. Am. Chem. Soc.* **2007**, *129*, 10754–10762. (b) Hill, S.; Edwards, R. S.; Aliaga-Alcalde, N.; Christou, G. *Science* **2003**, *302*, 1015–1018.

(6) Waldmann, O. *Inorg. Chem.* **2007**, *46*, 10035.

(7) Palii, A. V.; Ostrovsky, S. M.; Klokishner, S. I.; Tsukerblat, B. S.; Galán-Mascarós, J. R.; Berlinguette, C. P.; Dunbar, K. R. *J. Am. Chem. Soc.* **2004**, *126*, 16860. (a) Tsukerblat, B. S.; Palii, A. V.; Ostrovsky, S. M.; Kunitsky, S. V.; Klokishner, S. I.; Dunbar, K. R. *J. Chem. Theory Comput.* **2005**, *1*, 668. (b) Palii, A. V.; Ostrovsky, S. M.; Klokishner, S. I.; Tsukerblat, B. S.; Dunbar, K. R. *Chem. Phys. Chem.* **2006**, *7*, 871. (c) Ostrovsky, S. M.; Klokishner, S. I.; Palii, A. V.; Dunbar, K. R. *J. Mol. Struct.* **2007**, *838*, 138. (d) Klokishner, S. I.; Ostrovsky, S. M.; Palii, A. V.; Dunbar, K. *J. Mol. Struct.* **2007**, *838*, 133. (e) Palii, A. V.; Ostrovsky, S. M.; Klokishner, S. I.; Tsukerblat, B. S.; Schelter, E. J.; Prosvirin, A. V.; Dunbar, K. R. *Inorg. Chim. Acta* **2007**, *360*, 3915–3924.

(8) Atanasov, M.; Comba, P.; Daul, C. A. *Inorg. Chem.* **2008**, *47*, 2449. (a) Atanasov, M.; Busche, C.; Comba, P.; Hallak, F. E.; Martin, B.; Rajaraman, G.; Slageren, J. V.; Wadepohl, H. *Inorg. Chem.* **2008**, *47*, 8112–8125. (b) Atanasov, M.; Comba, P.; Daul, C. A. *J. Phys. Chem. A.* **2006**, *110*, 13332. (c) Atanasov, M.; Daul, C.; Güdel, H.-U. *Computational Chemistry: Reviews of Current Trends*; World Scientific: Singapore, 2005; Vol. *9*, pp 153−194.

(9) Mironov, V. S.; Chibotaru, L. F.; Ceulemans, A. *J. Am. Chem. Soc.* **2003**, *125*, 9750–9760.

(10) Beltran, L. M. C.; Long, J. R. *Acc. Chem. Res.* **2005**, *38*, 325.

(11) Miyasaka, H.; Matsumoto, N.; Okawa, H.; Re, N.; Gallo, E.; Floriani, C. *Angew. Chem., Int. Ed. Engl.* **1995**, *34*, 1446.

(12) Miyasaka, H.; Matsumoto, N.; Okawa, H.; Re, N.; Gallo, E.; Floriani, C. *J. Am. Chem. Soc.* **1996**, *118*, 981.

(13) Miyasaka, H.; Matsumoto, N.; Re, N.; Gallo, E.; Floriani, C. *Inorg. Chem.* **1997**, *36*, 670.

(14) Miyasaka, H.; Ieda, H.; Matsumoto, N.; Re, N.; Crescenzi, R.; Floriani, C. *Inorg. Chem.* **1998**, *37*, 255.

(15) Miyasaka, H.; Ieda, H.; Matsumoto, N.; Sugiura, K.; Yamashita, M. *Inorg. Chem.* **2004**, *42*, 3509.

clusters. For this field of study to progress, the electronic structure of these systems needs to be well-defined, and this is the primary objective of the current study. INS spectra, replete with detail, provide direct information on the low-energy levels of the MnCrMn and MnFeMn trimers, complementing new magnetic, calorimetric, and crystallographic data. The task of finding a self-consistent description is greatly assisted by the synthesis and characterization of the cobalt(III) analogue (MnCoMn). Given the strength of the experimental data and the limitations of the molecular field model, we provide a sober assessment of the function of these compounds as SMMs.

2. Experimental Section

2.1. Synthesis. The MnCrMn and MnFeMn trimers were synthesized by the addition of solutions of $K_3[Cr(CN)_6]$ and $K_3[Fe(CN)_6]$, respectively, to a solution of $[Mn(5\text{-}Brsalen)(H_2O)_2]ClO_4$, as described in ref 25. Fast addition of the two solutions gave products whose powder diffraction patterns were in accordance with the theoretical patterns of MnCrMn and MnFeMn, calculated from the structural data reported.[25] The diffractogram for MnCoMn exhibits peaks at similar positions and with similar intensities to those of the iron and chromium analogues, indicating that the three compounds are isostructural. Anal. calcd for $C_{38}H_{32}Br_4CoKMn_2N_{10}O_8$ (MnCoMn): C, 35.54; H, 2.51; N, 10.91. Found: C, 35.29; H, 2.29; N, 11.13. Anal. calcd for $C_{38}H_{32}Br_4CrKMn_2N_{10}O_8$ (MnCrMn): C, 35.73; H, 2.53; N, 10.97. Found: C, 36.12; H, 2.40; N, 11.60. Anal. calcd for $C_{38}H_{32}Br_4FeKMn_2N_{10}O_8$ (MnFeMn): C, 35.63; H, 2.52; N, 10.93. Found: C, 35.76; H, 2.35; N, 10.56.

Attempts to obtain crystals of larger dimensions by slow addition of the cyanometallate solution tended to result in dark-brown products with differing magnetic properties and powder diffraction patterns. The nature of these products was not investigated.

2.2. Powder X-Ray Diffraction Measurements. Variable-temperature high-resolution X-ray powder diffraction measurements were carried out at the powder diffraction station of the Materials Sciences Beamline, located at the Swiss Light Source, Paul Scherrer Institute, Switzerland. Data were collected in the high-resolution mode (a setup with the analyzer-crystal detector), and low temperatures were achieved with the use of the flow-type Janis cryostat. The powdered sample was enclosed in a 0.3-mm-diameter glass capillary, and the diffraction patterns in the angular range of typically 0−30° were obtained with an incident photon wavelength of ∼0.618 Å. The instrument resolution parameters were determined in a separate run on a standard sample in exactly the same geometry. The refinements of the crystal structure parameters were carried out with the program FullProf.[26]

2.3. Acquisition and Analysis of Neutron Diffraction Data. Between 2 and 3 g of powdered material was loaded into a 10-mm-diameter double-well hollow aluminum measurement cylinder, sealed under a He atmosphere to facilitate heat conduction. INS measurements were carried out on the direct time-of-flight spectrometer, FOCUS; the inverted-geometry time-of-flight spectrometer, MARS; and the powder diffractometer, DMC, all located at the Paul Scherrer Institute, and on the direct time-of-flight spectrometer, IN5, at the Institut Laue Langevin, Grenoble, France. All experiments utilized a standard ILL Orange cryostat for temperature control. For the FOCUS and IN5 experiments, an empty aluminum can of the same dimensions as the sample holder was measured and the spectrum subtracted from that of the sample; the detector efficiency correction was performed using data collected from vanadium. The FOCUS and MARS data were reduced and analyzed using the DAVE[27] (Data Analysis and Visualization Environment) program package. The IN5 data were reduced using LAMP[28] with subsequent analysis using DAVE. Measurements were undertaken at different instrumental settings, further details for which may be found in the figure captions pertaining to the experiment.

2.4. Magnetic Measurements. All magnetic measurements were conducted on a Quantum-Design MPMS-XL SQUID magnetometer, at the Department of Chemistry, University of Berne. Samples (10−20 mg) were wrapped in Saran film (3−6 mg) and suspended by a cotton thread in a standard SQUID straw. Measurements of the DC magnetic susceptibility were conducted with fields of 0.1 and 0.5 T at temperatures between 1.8 and 300 K. At least three different samples from each compound were measured both as powders and as compressed pellets to verify the reproducibility of the data.

2.5. Heat Capacity Measurements. Heat capacity measurements were carried out on a Quantum Design PPMS located at the PSI, Villigen. For samples of MnCoMn and MnFeMn, measurements were undertaken on compressed pellets with Apiezon grease as the thermal contact. The grease was measured prior to each measurement, over the same temperature range, and the values subsequently subtracted. Attempts to obtain data for MnCrMn using this procedure were not successful. Instead, data were obtained on a powdered sample mixed with Apiezon grease. This method was sufficient to check for prominent phase transitions, but the molar heat capacity could not be reliably determined.

3. Calculation of the Magnetic Properties and Neutron Scattering Spectra

3.1. Magnetic Data. All of the theoretical curves presented were calculated using *MagProp*,[29] a new program for the workup, visualization, and modeling of magnetic data and transition energies that is freely available. The magnetic moment per ion was calculated from the expression

(16) Ferbinteanu, M.; Hitoshi, Miyasaka, H.; Wernsdorfer, W.; Nakata, K.; Sugiura, K.; Yamashita, M.; Coulon, C.; Clérac, R. *J. Am. Chem. Soc.* **2005**, *127*, 3090.
(17) Miyasaka, H.; Saitoh, A.; Abe, S. *Coord. Chem. Rev.* **2007**, *251*, 2622.
(18) Berlinguette, C. P.; Vaughn, D.; Cañada-Vilalta, C.; Galán-Mascarós, J.-R.; Dunbar, K. R. *Angew. Chem., Int. Ed.* **2003**, *42*, 1523–1526.
(19) Van Langenberg, K.; Batten, S. R.; Berry, K. J.; Hockless, D. C. R.; Moubaraki, B.; Murray, K. S. *Inorg. Chem.* **1997**, *36*, 5006.
(20) Kaneko, W.; Kitagawa, S.; Ohba, M. *J. Am. Chem. Soc.* **2007**, *129*, 248.
(21) Yanai, N.; Kaneko, W.; Yoneda, K.; Ohba, M.; Kitagawa, S. *J. Am. Chem. Soc.* **2007**, *129*, 3496.
(22) Entley, W. R.; Girolami, G. S. *Inorg, Chem.* **1994**, *33*, 5165. (a) Franz, P.; Ambrus, C.; Hauser, A.; Chernyshov, D.; Hostettler, M.; Hauser, J.; Keller, L.; Krämer, K.; Stoeckli-Evans, H.; Pattison, P.; Bürgi, H.-B.; Decurtins, S. *J. Am. Chem. Soc.* **2004**, *126*, 2004.
(23) Palii, A. V.; Ostrovsky, S. M.; Klokishner, S. I.; Tsukerblat, B. S.; Dunbar, K. R. *ChemPhysChem.* **2006**, *7*, 871–879.
(24) Mironov, V. S. *Dokl. Phys. Chem.* **2007**, *415*, 199–204.
(25) Choi, H. J.; Sokol, J. J.; Long, J. R. *Inorg. Chem.* **2004**, *43*, 1606.
(26) Rodriguez-Carvajal, J. *Physica B* **1993**, *192*, 55.
(27) Azuah, R.; Copley, J.; Dimeo, R.; Park, S.; Lee, S.-H.; Munter, A.; Kneller, L.; Qiu Y.; Peral, I.; Brown, C.; Kienzle, P.; Tregenna-Piggott, P. L. W. *Dave 1.4 Beta*. http://www.ncnr.nist.gov/dave (accessed Nov 2008).
(28) LAMP, the Large Array Manipulation Program. http://www.ill.fr/data_treat/lamp/lamp.html (accessed Nov 2008).
(29) MagProp by Philip L. W. Tregenna-Piggott, available under DAVE.

$$M_{\text{ion}} = \frac{\sum_n \left(-\frac{dE_n}{dB}\right) \exp(-E_n/kT)}{\sum_n \exp(-E_n/kT)} \quad (1)$$

and the molar susceptibility from

$$\chi_M = N_A \frac{M_{\text{ion}}}{B} \quad (2)$$

In these equations, B designates the external magnetic field, k_B the Bolzmann constant, and N_A Avogadro's number. The sum is over the n eigenstates of the Hamiltonian whose energies are designated by the symbol E_n. The derivative in eq 1 was found according to the Hellman-Feynman theorem:

$$\frac{dE_n}{dB} = \langle \psi_n | \frac{d\hat{H}}{dB_0} | \psi_n \rangle \quad (3)$$

The nature of the states was revealed by calculating the expectation values of the $\hat{S}_z$ and $\hat{S}^2$operators.

3.2. INS Data. Henceforth, we use the numeration of the metal ions shown in Scheme 1.

The intensity of neutrons being magnetically scattered according to the geometry defined by the incoming wavevector $\mathbf{k}_i$ and outgoing wavevector $\mathbf{k}_f$ is proportional to[30]

$$I \propto \frac{k_f}{k_i} p_\sigma p_\lambda |\langle \lambda' \sigma' | F_1(Q) \exp(i\mathbf{Q}\cdot\mathbf{R}_1)\, \hat{\sigma}\cdot\hat{\mathbf{Q}}_{1\perp} + F_2(Q) \exp(i\mathbf{Q}\cdot\mathbf{R}_2)\, \hat{\sigma}\cdot\hat{\mathbf{Q}}_{2\perp} + F_3(Q) \exp(i\mathbf{Q}\cdot\mathbf{R}_3)\, \hat{\sigma}\cdot\hat{\mathbf{Q}}_{3\perp} | \lambda\sigma \rangle|^2 \quad (4)$$

where k_f and k_i are the lengths of $\mathbf{k}_f$ and $\mathbf{k}_i$, respectively, and $\mathbf{Q} = \mathbf{k}_f - \mathbf{k}_i$ is the scattering vector with length Q; F_1, F_2, and F_3 are the magnetic form factors for ions 1, 2, and 3 with position vectors $\mathbf{R}_1$, $\mathbf{R}_2$, and $\mathbf{R}_3$. In a pure spin model, the operator $\hat{\mathbf{Q}}_{1\perp}$ may be expressed as $\hat{\mathbf{Q}}_{1\perp} = 1/Q^2(Q \times \hat{\mathbf{S}}_1 \times Q)$. p_λ is the thermal population of the spin-system level λ; p_σ is the population of neutron state σ. $\hat{\boldsymbol{\sigma}}$ is the neutron spin operator. As the experiments were performed with unpolarized neutrons on powdered samples, eq 4 was summed for all four possible combinations of entering and leaving neutron spins and powder averaged. As written, eq 4 accounts for the intensity caused by a single transition $\lambda \rightarrow \lambda'$. The total intensity is obtained by summing over all initial and final states. The MnFeMn system is not strictly a spin-only system. However, we use eq 4 also for this system, assuming that the effect of orbital angular momentum of Fe(III) may be absorbed in the form factor.

4. Results and Discussion

4.1. The Structure of MnCrMn. Variable-temperature high-resolution X-ray powder diffraction measurements were carried out on MnCrMn, motivated by the anomalous magnetic data collected at low temperatures. Diffractograms collected at 5, 20, and 298 K presented in Figure S1 (Supporting Information) are in very close correspondence.

(30) *Introduction to the Theory of Thermal Neutron Scattering, by Squires*; G. L. Dover Publications, Inc: Mineola, NY, 1996.

Scheme 1. Metal Skeletons of the $K[(5\text{-Brsalen})_2(H_2O)_2\text{-}Mn_2M(CN)_6]\cdot 2H_2O$ Clusters (M = Co(III), Cr(III), Fe(III)), and Numeration of the Ions

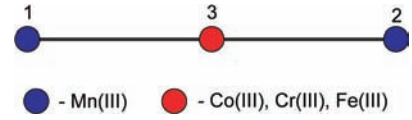

Rietveld refinements were performed on all three patterns, using the coordinates published in ref 25 as a starting point. The 5 K experimental and model powder patterns are presented in Figure S2 (Supporting Information) and are seen to be in good agreement. All three structures differ little from that previously reported from a room-temperature single-crystal X-ray study. The diffractograms and CIF files are included as Supporting Information. Since the MnCrMn structural unit has been discussed previously,[25] we confine our discussion to the intertrimer bonding, which we deem to be crucial in understanding the magnetic properties of these systems. The following figures and bond lengths are derived from the structure determined from the 5 K powder diffraction data.

The arrangement of the trimers in the *bc* plane is presented in Figure S3 (Supporting Information) along with selected bond distances between transition metal ions of different trimers. The bond distance between managanese(III) cations lying head-to-tail in the *bc* plane is 5.089(7) Å, while the distance between the manganese(III) and chromium(III) cations of trimers situated adjacently is 6.730(4) Å. The distances, though too large to facilitate direct exchange of any significance, are small enough to warrant consideration of intertrimer superexchange interactions within the *bc* plane.

Figure S4 (Supporting Information) represents an expanded view of the region in Figure S3 within the area marked by an oval. The manganese(III) cations situated head-to-tail are separated by two water molecules. The distance between the oxygen atoms is 3.99(2) Å, which is too long for consideration of a hydrogen bond of any significance. A less tortured superexchange pathway is identified between the manganese(III) and chromium anion. The distance between the oxygen and nitrogen atoms is 2.88 Å, typical of a weak O−H···N hydrogen bond. On the basis of the structural data, therefore, we conclude that a small but non-negligible exchange interaction between the trimers in the *bc* plane is possible. No other viable intertrimer superexchange pathways have been identified. Note that the packing is analogous to that documented for the $(NEt_4)[Mn_2(salmen)_2(MeOH)_2\text{-}Fe(CN)_6]$ trimer, for which SMM properties have been verified,[16] but the trimeric units in the 5-Brsalen compounds are in closer proximity on account of crystallizing with water rather than methanol units. A greater intertrimer exchange interaction for the 5-Brsalen compounds can therefore be expected.

4.2. INS, Magnetic Susceptibility, and Magnetisation Measurements of MnCoMn. An INS spectrum for MnCoMn recorded at 15 K is presented in Figure 2. Further data extending to lower energies and higher temperatures are presented in Figures S5 and S6 of the Supporting Information. At 1.5 K, a single peak is located at ~11.6 cm^{-1}.

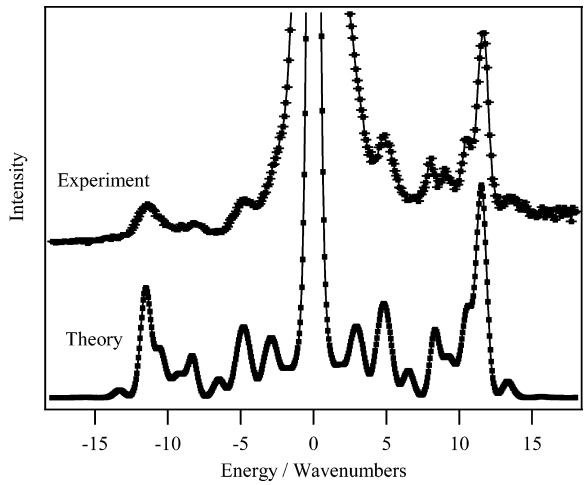

Figure 2. Experimental and theoretical INS spectra of MnCoMn, measured and calculated at 15 K. The experimental spectrum was recorded on FOCUS with an incident wavelength of 4.85 Å. The instrumental resolution at both 0 cm^{-1} and 16 cm^{-1} is ~0.8 cm^{-1}. The theoretical spectrum was calculated using eqs 4 and 5 with the parameters $D = -3.5$ cm^{-1}, $E/D = 0.057$ and $J_{12} = 0.63$ cm^{-1}.

As the temperature is increased, the intensity of this peak diminishes, concomitant with the emergence of a number of peaks at lower energy. The complexity of the spectrum at 15 K is inconsistent with spectra observed for a mononuclear manganese(III) cation[31] but can be explained allowing for a small antiferromagnetic interaction between the two manganese(III) cations of a given trimer.

The lower trace in Figure 2 is a theoretical spectrum calculated from the spin-Hamiltonian

$$\hat{H} = D\sum_{1,2}\left(\hat{S}_{iz}^2 - \frac{1}{3}S_i(S_i+1)\right) + E\sum_{1,2}(\hat{S}_{ix}^2 - \hat{S}_{iy}^2) + \mu_B\sum_{1,2} B\cdot g\cdot\hat{S}_i + J_{12}\hat{S}_1\cdot\hat{S}_2 \quad (5)$$

where the indices 1 and 2 run over the manganese(III) cations (Scheme 1), each of spin $S = 2$. The last term in eq 5 describes the exchange interaction between the two manganese(III) cations mediated by the diamagnetic cobalt(III) ion, which in a sense plays the role of a bridging ligand. The spectrum was calculated using the parameters $D = -3.5$ cm^{-1}, $E/D = 0.057$, and $J_{12} = 0.63$ cm^{-1} and is seen to be in excellent agreement with experimental results. The single ion anisotropy is consistent with values determined for other manganese(III) centers subject to similar coordination environments.[32] The exchange coupling constant is, as expected, very small but has a significant effect on the INS spectrum.

In Figure 3 are shown magnetic susceptibility data, displayed as $\chi_m T$ in the 1.8−300 K temperature range. Overlaid is a red curve calculated using the Hamiltonian in eq 5 that is seen to give an impressive reproduction of the

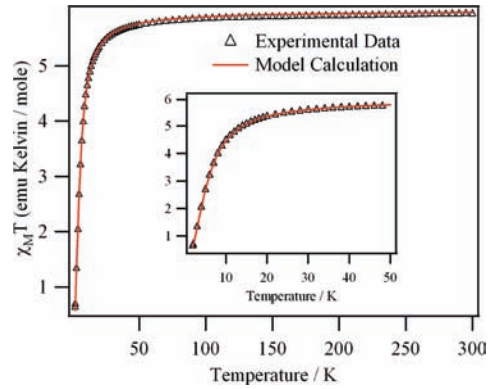

Figure 3. Variation of χT versus temperature, measured and calculated for MnCoMn. The model curve was calculated from the Hamiltonian given in eq 5, with $g = 2.0$, $D = -3.5$ cm^{-1}, $E/D = 0.057$, and $J_{12} = 0.63$ cm^{-1}.

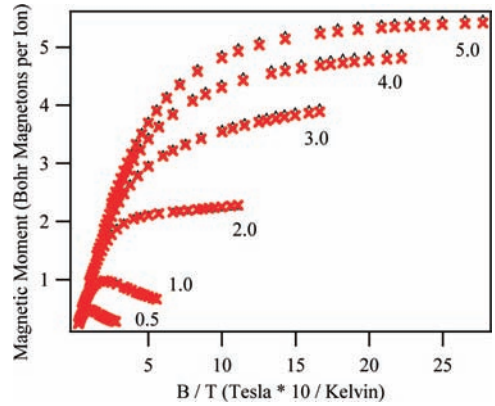

Figure 4. Variation of the magnetic moment of MnCoMn as a function of *B*/*T* (black triangles), for various fields as indicated on the figure. The model curve (red crosses) was calculated from the Hamiltonian given in eq 5, with the same parameters as given in the caption of Figure 3.

experimental data. The parameters used for the calculation are once again $g = 2.0$, $D = -3.5$ cm^{-1}, $E/D = 0.057$, and $J_{12} = 0.63$ cm^{-1}, in keeping with the value determined from the INS spectra. These parameters also provide an excellent account of magnetization data collected at high fields and low temperatures, as seen in Figure 4.

The study of MnCoMn shows that the single ion anisotropy of the manganese(III) center is well described by setting the second-order zero-field-splitting parameters *D* and *E*/*D* to -3.5 cm^{-1} and 0.057, respectively. Though the available crystallographic data identify small structural differences about the manganese(III) center,[25] a significant variation of the single ion anisotropy in the MnCoMn, MnCrMn, and MnFeMn trimers is not to be expected. On the basis of the MnCoMn data, a small exchange coupling between the manganese(III) cations could also be anticipated for MnCrMn and MnFeMn. However, in the subsequent analysis, we show that a satisfactory account of the data can be obtained with this parameter set to zero.

4.3. INS and Magnetic Susceptibility Measurements of MnCrMn. In Figure 5 are presented variable-temperature INS spectra of the MnCrMn trimer. At 1.5 K, two cold peaks are identified at 13.5 and 23.0 cm^{-1}, labeled I and II, respectively, with the higher energy transition notably broader. Spectra between 6 and 15 K exhibit additional peaks

(31) Basler, R.; Tregenna-Piggott, P. L. W.; Andres, H.-P.; Dobe, C.; Güdel, H.-U.; Janssen, S.; McIntyre, G. J. *J. Am. Chem. Soc.* **2001**, *123*, 3377–3378. (a) Scheifele, Q.; Riplinger, C.; Neese, F.; Weihe, H.; Barra, A.-L.; Juranyi, F.; Podlesnyak, A.; Tregenna-Piggott, P. L. W. *Inorg. Chem.* **2008**, *47*, 439–447.

(32) Kennedy, B. J.; Murray, K. S. *Inorg. Chem.* **1985**, *24*, 1552. (a) Krzystek, J.; Telser, J. *J. Magn. Reson.* **2003**, *162*, 454–465.

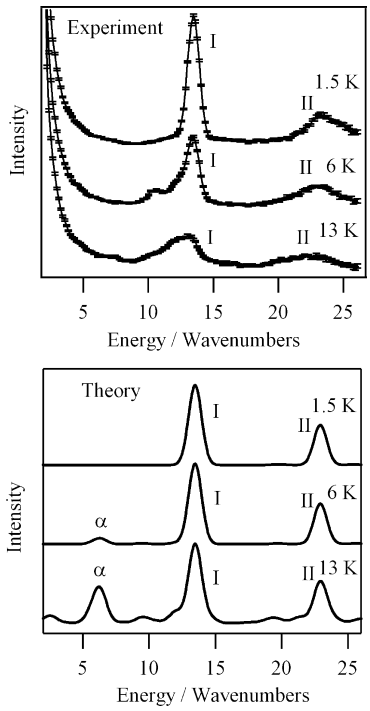

Figure 5. Experimental and theoretical INS spectra of MnCrMn as a function of the temperature. The experimental spectra were recorded on FOCUS with an incident wavelength of 4.4 Å. The instrumental resolutions at 0 cm^{-1} and 16 cm^{-1} are ~1.7 cm^{-1} and ~1.0 cm^{-1}, respectively. The theoretical spectra were calculated using eq 6 with the parameters $D = -4.0$ cm^{-1}, $E/D = 0.057$, $J_{13\_23} = 8.5$ cm^{-1}, and $J_{int} = 0.00$ cm^{-1}. J_{int} is the characteristic parameter of the intercluster interaction (see eqs 11 and 12).

at lower energy, seen most clearly in the higher-resolution spectra presented in Figure S7 (Supporting Information). All peaks broaden significantly upon warming to 13 K, and the spectrum is not readily discerned at higher temperatures.

To model the experimental data for MnCrMn, the Hamiltonian in eq 5 must now be expanded to include the paramagnetic Cr(III) center:

$$\hat{H}_{mol} = D\sum_{1,2}\left(\hat{S}_{iz}^2 - \frac{1}{3}S_i(S_i+1)\right) + E\sum_{1,2}(\hat{S}_{ix}^2 - \hat{S}_{iy}^2) + \mu_B\sum_{1,2,3} B\cdot g\cdot\hat{S}_i + J_{13\_23}(\hat{S}_1\cdot\hat{S}_3 + \hat{S}_2\cdot\hat{S}_3) \quad (6)$$

where the Cr(III) cation has the spin $S_3 = 3/2$. Furthermore, we exclude from consideration the exchange interaction of the Mn(III) ions within the cluster since, when the central ion in the cluster is paramagnetic, the exchange pathway Mn(III)−M(III) (M = Cr,Fe) is dominant.

A good reproduction of the experimental INS data is obtained with the parameters $D = -4.0$ cm^{-1}, $E/D = 0.057$, and $J_{13\_23} = 8.5$ cm^{-1}, as seen in Figure 5. It is difficult to say whether the small difference in the D parameter determined for the cobalt(III) and chromium(III) trimers is real or a consequence of the limitation of the model. With reference to the energy level diagram in Figure 6, the two cold peaks I and II are assigned to the transitions $M_s \sim \pm 2.5$ ($S = 5/2$) → $M_s \sim \pm 1.5$ ($S = 5/2$) and $M_s \sim \pm 2.5$ ($S = 5/2$) → ± 1.5 ($S = 3/2$). The three lowest Kramers doublets derive from an $S = 5/2$ ground state, whose splitting may be approximately described by the Hamiltonian

$$\hat{H}_s = D\left[\hat{S}^2 - \frac{1}{3}S(S+1)\right] \quad (7)$$

with $D \sim -3.6$ cm^{-1}. The next levels are microstates of an $S = 3/2$ spin state. Of the two cold peaks, the transition energy of peak II is far more sensitive to the value of the parameter J_{13_23}. The observation that peak II is considerably broader than peak I is therefore consistent with a distribution of values for the manganese−chromium exchange interaction about a mean value of 8.5 cm^{-1}.

Variable-temperature magnetic susceptibility data are presented in Figure 7. The blue curve results from least-squares refinement of the $\chi_m T$ values in the 100−300 K temperature range, as is seen to correlate well with the experimental data down to ~50 K. Below this temperature, the measured moment falls far more precipitously than predicted. We have found no explanation for the discrepancy other than the existence of antiferromagnetic intertrimer exchange interactions, the possible origin of which was discussed in section 4.1. At this juncture, we remind the reader of the fundamental approximation behind molecular-field theory. In the framework of the molecular-field approximation, the spin operator at the jth site is written in terms of the average value, $\bar{S}_j$, and the deviation (or fluctuation) from it:

$$\hat{S}_j = \bar{S}_j + (\hat{S}_j - \bar{S}_j) = \bar{S}_j + \partial\hat{S}_j \quad (8)$$

Provided that the fluctuations are small, the Heisenberg Hamiltonian may then be simplified as

$$\begin{aligned}\hat{H}_{Heisenberg} = -J\hat{S}_i\cdot\hat{S}_j &= -J\hat{S}_i\cdot(\bar{S}_j + \partial\hat{S}_j)\\ &= -J(\bar{S}_j\hat{S}_i + \hat{S}_i\cdot\partial\hat{S}_j)\\ &\sim -J\bar{S}_j\hat{S}_i\end{aligned} \quad (9)$$

Within this framework, the antiferromagnetic interaction can be readily treated by dividing the crystal into two magnetic sublattices, A and B,

$$\hat{H} = \sum_n \hat{H}_n^A + \sum_m \hat{H}_m^B \quad (10)$$

the Hamiltonians for which are written as

$$\hat{H}_n^A = \hat{H}_{mol}^n - J_{int}(\bar{S}_Z^B S_{Zn}^A + \bar{S}_X^B S_{Xn}^A + \bar{S}_Y^B S_{Yn}^A) \quad (11)$$

$$\hat{H}_m^B = \hat{H}_{mol}^m - J_{int}(\bar{S}_Z^A S_{Zm}^B + \bar{S}_X^A S_{Xm}^B + \bar{S}_Y^A S_{Ym}^B) \quad (12)$$

where n and m number the molecules in sublattices A and B, respectively. The first terms in eqs 11 and 12 denote the Hamiltonian of the molecule, given in eq 6, and the second term accounts for the antiferromagnetic interaction between the two sublattices. The expectation values for the spin-operators are calculated as

$$\overline{S_{Z,X,Y}^{A,B}} \equiv \langle\hat{S}_{Z,X,Y}^{A,B}\rangle = \frac{Tr(\exp[-E^{A,B}/kT]\langle\psi|\hat{S}_{Z,X,Y}^{A,B}|\psi\rangle)}{Tr(\exp[-E^{A,B}/kT])} \quad (13)$$

These quantities are found by an iterative, self-consistent procedure, and the total magnetic moment is found as the sum of the values calculated from eqs 11 and 12. Note that, since spin fluctuations are neglected, the mean field treatment provides but an upper limit for the strength of the intermo-

lecular interaction and the associated temperature of the magnetic phase transition. For a strictly two-dimensional Heisenberg model of intercluster exchange, no magnetic phase transition is expected.[33]

Least-square refinement of the INS transition energies and the $\chi_m T$ data in the 8−300 K temperature range for the corresponding quantities calculated from the model Hamiltonian (eq 10) yielded the parameters $D = -4.0$ cm^{-1}, $E/D = 0.057$, $J_{13\_23} = 8.5$ cm^{-1}, and $J_{int} = -1.0$ cm^{-1}. The theoretical $\chi_m T$ data, shown as the red curve in Figure 7, are seen to correspond well with the experimental data. Below ∼8 K, the mean-field calculation predicts that MnCrMn will enter into an antiferromagnetic ordered phase, the clearest manifestation of which would be the appearance of magnetic diffraction peaks as the sample is cooled through the phase transition. Inspection of the powder neutron diffraction data presented Figure S8 (Supporting Information) shows that this is not observed. Furthermore no anomaly is present in the $\chi_m T$ data presented in Figure 7 or in measurements of the specific heat capacity (not presented). The strength of the internal field between 2 and 8 K is predicted to be strongly dependent upon the temperature, as shown in the energy-level diagram presented in Figure S9 (Supporting Information), which would result in a notable shift in the positions of the calculated INS peaks as shown in Figure S10 (Supporting Information). Although the energy of transition II (Figure 5) is observed to decrease upon increasing the temperature, the reduction is less than that calculated, and no change in the position of transition I can be reliably established. Finally, we have been unable to find a set of parameters that can adequately describe magnetization data in this temperature range (Figure S11, Supporting Information).

Since the experimental data fail to identify a phase transition, the magnetic data collected below 8 K cannot be analyzed within the confines of the molecular-field approximation. It is for this reason that the magnetic data were analyzed down to 8 K only, and the internal field resulting from the predicted phase transition was neglected in the calculated INS spectra presented in Figure 5. Note that the model does not provide a convincing account of the variation of the INS spectra with temperature. This would suggest that the model is incomplete, but the introduction of further terms does not lead to a significant improvement. Certainly, it is not possible to reproduce the fine structure evident in the spectra presented in Figure S7 (Supporting Information) with just one set of parameters.

4.4. INS, Magnetic Susceptibility, and Magnetisation Measurements of MnFeMn. INS spectra displayed in Figure 8 exhibit two prominent cold peaks at ∼11.5 and ∼15 cm^{-1}, labeled I and II, respectively. Upon warming from 2 to 6 K, a hot band emerges at ∼9 cm^{-1}. At ∼15 K, the peaks are considerably broader, and at 30 K (Figure S12, Supporting Information), the spectral features cannot be distinguished from the baseline.

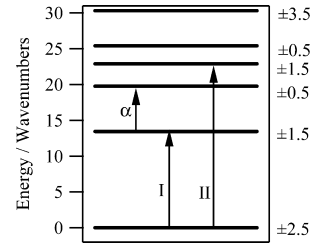

Figure 6. Energy level diagram pertaining to MnCrMn, calculated with the parameters used to calculate the theoretical INS spectrum given in the caption of Figure 5. The states are labeled according to the expectation value of the operator, $\hat{S}_z$.

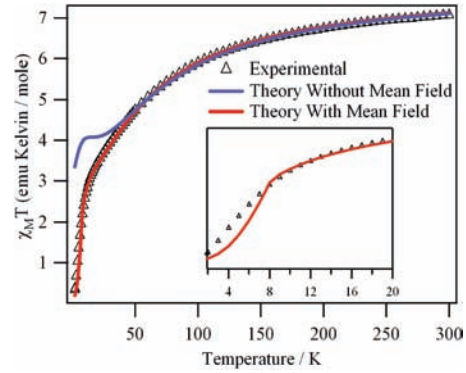

Figure 7. Variation of $\chi_M T$ versus temperature, measured and calculated for MnCrMn. The model curve was calculated from the Hamiltonian given in eqs 6 and 10, with $D = -4.0$ cm^{-1} and $E/D = 0.057$, the values used to model the INS data. The **g** matrix was assumed to be isotropic and was assigned a value of 2.0. The data were fitted with and without a mean field theory correction, as indicated in the figure. The blue curve was calculated by least-squares fitting of the data from 100 to 300 K with J_{int} set to zero, from which a value for J_{13_23} of ∼11 cm^{-1} was obtained. The red curve was obtained by least-squares fitting of the magnetic data from 8 to 300 K and the INS transition energies, from which J_{13_23} was determined to be 8.5(12) cm^{-1} and $J_{int} = -1.0(2)$ cm^{-1}.

Both peaks are asymmetric, and high-resolution IN5 and MARS spectra presented in Figures S13−S15 (Supporting Information) indicate that peaks I and II are in fact doublets, with components of approximately equal intensity. Analysis of the IN5 data confirms that the relative intensity of the doublets comprising the cold peak at ∼11.5 cm^{-1} is independent of momentum transfer, Q, suggesting that the appearance of the doublet in the powder-averaged spectrum is not a consequence of dispersion.

The variation of $\chi_m T$ versus temperature is presented in Figure 9. The value of $\chi_m T$ rises gradually upon cooling from 300 K to ∼20 K, in accordance with the ferromagnetic interaction between the manganese(III) and iron(III) cations documented earlier,[12] and then falls precipitously upon cooling further to 2 K, indicative once more of antiferromagnetic exchange interactions between the trimers.

The first step to modeling the data is to obtain a reasonable estimate of the energy spectrum of the $[Fe(CN)_6]^{3-}$ anion in this crystallographic environment. In a recent paper by Atanasov and co-workers,[34] estimates for the angular overlap model (AOM) bonding parameters of the $[Fe(CN)_6]^{3-}$ anion

(33) Mermin, N. D.; Wagner, H. *Phys. Rev. Lett.* **1966**, *17*, 1133.

(34) Atanasov, M.; Comba, P.; Daul, C. A.; Hauser, A. *J. Phys. Chem. A* **2007**, *111*, 9145–9163.

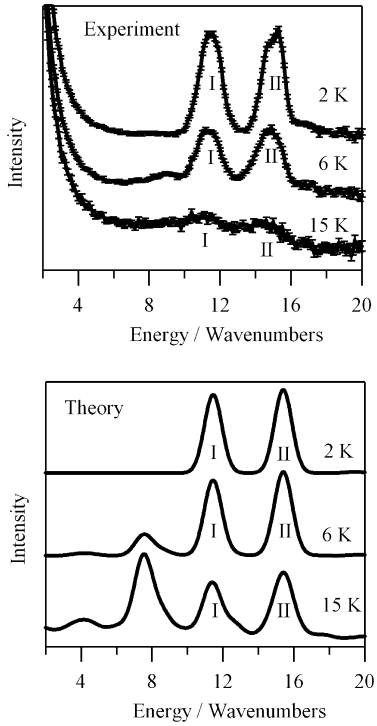

Figure 8. Experimental and theoretical INS spectra of MnFeMn as a function of the temperature. The experimental spectra were recorded on FOCUS with an incident wavelength of 4.85 Å. The instrumental resolutions at 0 cm^{-1} and 16 cm^{-1} are ~1.4 cm^{-1} and ~0.6 cm^{-1}, respectively. The theoretical spectra were calculated with the parameters $D = -4.0$ cm^{-1} and $E/D = 0.057$, $J^{x,y}_{13\_23} = -5.7$ cm^{-1}, $J_{13\_23} = -6.9$ cm^{-1}, and $J_{int} = 0.0$ cm^{-1}.

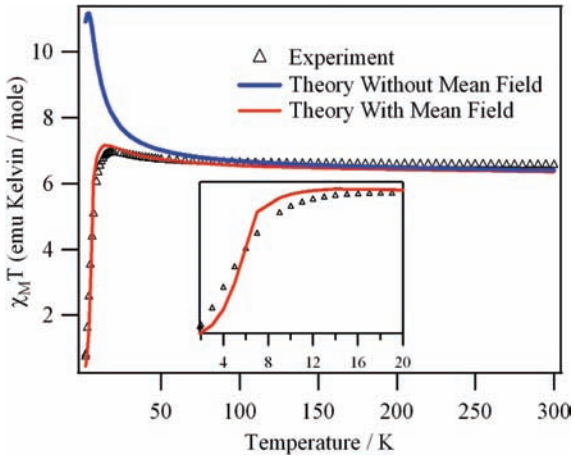

Figure 9. Variation of $\chi_M T$ versus temperature, measured and calculated for MnFeMn. The red curve was obtained by least-squares fitting of the magnetic data from 8 to 300 K and the INS transition energies. The model curve marked in red was calculated from the Hamiltonian given in eqs 10 and 14, with $D = -4.0$ cm^{-1} and $E/D = 0.057$, $J^{x,y}_{13\_23} = -5.7$ cm^{-1}, $J_{13\_23} = -6.9$ cm^{-1}, and $J_{int} = -0.31$ cm^{-1}. These values were obtained by least-squares fitting of the magnetic data from 8 to 300 K and the INS transition energies. The model blue curve was calculated with the same parameters but with J_{int} set to zero.

were obtained by modeling the results of ligand-field density functional theory calculations, in conjunction with experimental data from the $K_3Fe(CN)_6$ salt. Adapting these parameters to the structure of the $[Fe(CN)_6]^{3-}$ anion within the MnFeMn trimer, and assuming that the spin−orbit coupling and Racah parameters are reduced to 75% of their free-ion values, AOM calculations undertaken using LIG-

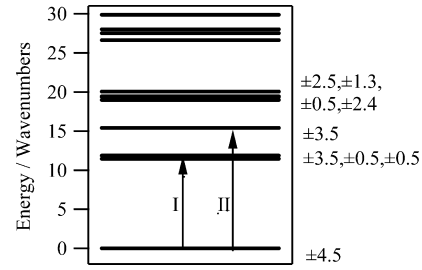

Figure 10. Energy level diagram pertaining to MnFeMn, calculated with the parameters used to calculate the theoretical INS spectrum given in the caption of Figure 8. The states are labeled according to the expectation value of the operator, $\hat{S}_z$, representing the sum of the Mn(III) $S = 2$ spins and the $S = 1/2$ pseudospin of the Fe(III) ion.

FIELD[35] suggest that the $^2T_{2g}$ ground term splits into Kramers doublets with energy separations of 0, 590, and 1007 cm^{-1}. The ground-state g values are calculated as $g_z = 2.26$, $g_y = 2.16$, and $g_x = 2.00$. Thus, we arrive at the conclusion that the ground Kramers doublet is well-separated from the excited ones, and the $[Fe(CN)_6]^{3-}$ anion can be described as possessing a pseudospin of 1/2. The exchange interaction of the Fe(III) ion and the Mn(III) ions may be highly anisotropic due to orbitally dependent contributions,[8,19] and within the ground Kramers doublet of the Fe(III) interacting with the Mn(III) ions, we write the Hamiltonian of the whole cluster in the following form:

$$\hat{H}_{mol} = D\sum_{1,2}\left(\hat{S}^2_{iz} - \frac{1}{3}S_i(S_i+1)\right) + E\sum_{1,2}(\hat{S}^2_{ix} - \hat{S}^2_{iy}) + \mu_B\sum_{1,2,3} B\cdot g\cdot\hat{S}_i + J^z_{13\_23}(\hat{S}_{1z}\hat{S}_{3z} + \hat{S}_{2z}\hat{S}_{3z}) + J^{x,y}_{13\_23}(\hat{S}_{1x}\hat{S}_{3x} + \hat{S}_{2x}\hat{S}_{3x} + \hat{S}_{1y}\hat{S}_{3y} + \hat{S}_{2y}\hat{S}_{3y}) \quad (14)$$

where $S_1 = S_2 = 2$ and $S_3 = 1/2$ is the pseudospin of the Fe(III) ion; $S_{3\alpha}(\alpha = x, y, z)$ are the projections of the pseudospin S_3.

The INS spectra may be reproduced with the parameters, $D = -4.0$ cm^{-1}, $E/D = 0.057$, $J_{13\_23} = -6.9$ cm^{-1}, and $J^{x,y}_{13\_23} = -5.7$ cm^{-1}, as seen in Figure 8. The energy level diagram, derived from modeling the INS data, is presented in Figure 10. The ferromagnetic manganese(III)−iron(III) interaction, in conjunction with the single ion anisotropy of the Mn(III) centers, results in a ground-state Kramers doublet with the expectation value $M_s \sim \pm 9/2$. The energy spectrum up to ~30 cm^{-1} is awash with levels derived from different S manifolds, mixed via the anisotropic terms in the Hamiltonian. Transitions I and II are assigned as the $M_s \sim \pm 4.5$ ($S = 9/2$) → $M_s \sim \pm 3.5$ ($S = 9/2$) and $M_s \sim \pm 4.5$ ($S = 9/2$) → $M_s \sim \pm 3.5$ ($S = 7/2$) transitions. The experimental spectra are of high quality, despite being recorded on a sample rich in hydrogen, and the intensity of the two cold peaks, I and II, may be reasonably well determined as a function of momentum transfer, Q, as shown in Figure S16 (Supporting Information). The observed oscillations reflect the wave functions of the states, between which the transition occurs, and the spatial separation of the metal centers.[36] The variations of the intensities of transitions I and II with

(35) Bendix, J. *Comp. Coord. Chem. II* **2004**, *2*, 673–676.

increasing Q are well reproduced by the theoretical curves, lending credence to the model.

The variation of $\chi_m T$ versus temperature may be reproduced with the same parameters but once again only by allowing for a small antiferromagnetic interaction that, within the confines of molecular field theory, is predicted to give rise to a magnetic phase transition at ~7 K. This is apparent from the model curve marked in red, presented in Figure 9, but is not consistent with the experimental data. By analogy with MnCrMn, powder neutron diffraction data presented in Figure S8 (Supporting Information) provide no hint of magnetic order down to 2 K. Measurements of the specific heat, displayed in Figure S17 (Supporting Information), do exhibit a broad bump at ~7 K that cannot be attributed to a Schottky anomaly (Figure S18, Supporting Information), but data collected on MnCoMn, included for comparison, appear to exhibit a similar anomaly at this temperature (Figure S17, Supporting Information). The energy level diagram (Figure S19, Supporting Information) and theoretical INS spectra (Figure S20, Supporting Information) arising from the molecular-field calculation are highly temperature-dependent, which once again is not supported by experimental results, and the fit to the magnetization data using this model is unconvincing (Figure S21, Supporting Information). As there is no evidence for a magnetic phase transition, magnetic data below ~7 K were not included in the analysis, and the internal field was neglected in the calculation on the INS spectra presented in Figure 8.

Note from the Hamiltonian written in eq 14 that we have imposed axial symmetry on the manganese(III)−iron(III) exchange interaction and have assumed the coordinate systems defining the single ion anisotropy and exchange interactions to be collinear. An improvement to the fits could no doubt be obtained by lifting these restrictions, but the data would be hopelessly parametrized. We can state only that it is necessary to introduce anisotropy in the iron(III)−manganese(III) exchange interaction to model the data satisfactorily but that $J^{z}_{13\_23}$ and $J^{x,y}_{13\_23}$ should be treated as effective parameters. We can proffer no explanation for the doubling of INS peaks I and II other than the existence of two distinct species, present in equal proportions.

4.5. AC Magnetic Susceptibility Measurements of MnCrMn and MnFeMn. Since no experimental evidence exists for magnetic order down to 2 K, we proceed to interpret the AC magnetic susceptibility data for MnCrMn and MnFeMn in terms of the energy-level diagrams derived for the isolated trimeric units.

The out-of-phase component of the susceptibility of MnCrMn is presented in the upper part of Figure 11 and is in excellent correspondence with that reported previously.[25] The dependence of the relaxation time, τ, upon temperature may be estimated from the peaks in the AC susceptibility data of MnCrMn. These data points conform to an Arrhenius

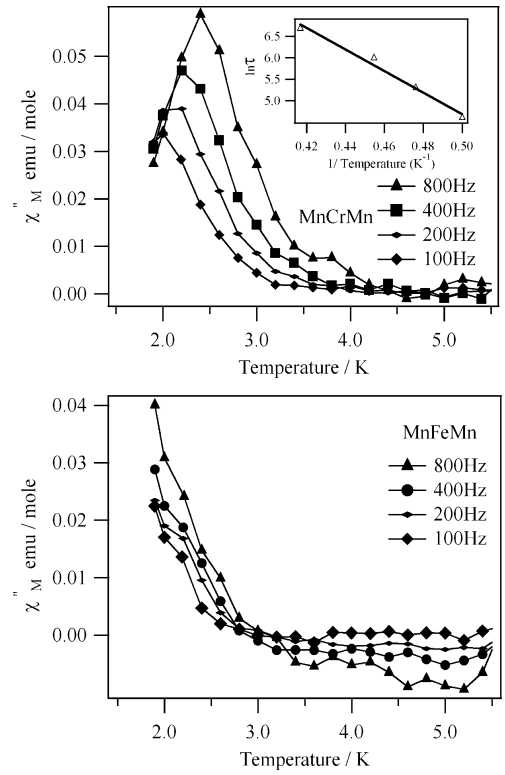

Figure 11. Temperature dependence of the out-of-phase components of the molar AC magnetic susceptibility for MnCrMn and MnFeMn, as measured in a 3G field oscillating at selected frequencies. The plot in the inset shows that the relaxation times, τ, obtained from the peaks in the AC susceptibility data of MnCrMn conform to an Arrhenius relationship from which an estimate to the spin-barrier of 17(2) cm^{-1} is derived.

relationship from which an estimate to the thermally activated barrier of 17(2) cm^{-1} is derived. This value does indeed correlate well with the energy difference between the $M_s = \pm 2.5$ and $M_s = \pm 0.5$ levels, as seen in energy level diagram presented in Figure 6.

All of the magnetic data we have collected on MnCrMn and MnFeMn are in good agreement with those reported by the group of Long,[25] with the exception of the AC susceptibility measurements on MnFeMn, which were the basis of their paper. By analogy to the MnCrMn data, these workers reported peaks in the out-of-phase susceptibility from which an estimate for the thermally activated barrier of 25 cm^{-1} was derived. Ferbinteanu and co-workers failed to reproduce these results and arrived at the conclusion that the MnFeMn cluster is not a SMM.[16] The data sets collected on the two samples of MnFeMn that we have prepared are consistent but are not in agreement with those previously reported. The out-of-phase component of the susceptibility displays the onset of peaks upon cooling to ~1.7 K, as shown in the lower part of Figure 11. It follows from Figure 10 that the ground state of the trimer possesses a maximum spin projection value $M_S = \pm 4.5$, thus indicating the presence of the spin reversal barrier. However, unlike the situation for MnCrMn, the energy pattern cannot be described by the simple dependence $E(M_S) = D_S M_S^2$, since the ground and excited spin multiplets are intertwined. In the absence of quantum tunnelling being active in the Arrhenius regime, a thermal barrier of at least ~11.5 cm^{-1} is to be expected, as

(36) (a) Waldmann, O. *Phys. Rev. B: Condens. Matter Mater. Phys.* **2005**, *71*, 094412. (b) Güdel, H. U. In *Magneto-Structural Correlations in Exchange-Coupled Systems*; Willet, R. D., Ed.; Reidel: Amsterdam, 1985, p 325. (c) Furrer, A.; Güdel, H. U. *J. Magn. Magn. Mater.* **1979**, *14*, 256.

this value corresponds to the energy difference between the ground $M_s = \pm 4.5$ Kramers doublet and the collection of first excited states of composition $M_s = \pm 3.5$, ± 0.5, and ± 0.5. Though the magnetization will relax once $M_s = \pm 0.5$ levels are thermally occupied, transitions from the $M_s = \pm 4.5$ to the $M_s = \pm 0.5$ states and from the $M_s = \pm 3.5$ to the $M_s = \pm 0.5$ states are forbidden to first order; only transitions from the $M_s = \pm 4.5$ to $M_s = \pm 3.5$ states are allowed. For this reason, it is not evident how many levels contribute to the barrier formation. To answer this question, one has to examine the relaxation pathways, and this work is in progress.

5. Summary

The electronic structures of MnCrMn and MnFeMn are highly complex due to the manganese(III) single ion anisotropy and intramolecular exchange coupling being comparable in magnitude, as well as the presence of weak intertrimer exchange coupling. The task of probing these interactions has been greatly facilitated by the application of a wide range of physical techniques and the synthesis and characterization of the MnCoMn analogue. The intratrimer exchange interactions of these compounds have been determined to a degree of certainty that goes well beyond that obtained from routine magnetic susceptibility measurements alone. In particular, we reaffirm that an anisotropic manganese(III)−iron(III) exchange interaction must be assumed to model adequately the INS and magnetic susceptibility data of MnFeMn, in accordance with previous theoretical predictions.[8,19] The antiferromagnetic intertrimer exchange coupling attenuates the magnetic moment of MnCrMn and MnFeMn at low temperatures, but there is no evidence for the onset of magnetic order in the 2−300 K temperature range for either of these compounds. The AC susceptibility data of MnCrMn suggest a spin-reversal barrier of 17(2) cm^{-1}, which is fully consistent with the energy-level diagram determined. MnFeMn also qualifies as a SMM, but the magnitude of the thermal barrier cannot be reliably established from the data we have collected. A rigorous characterization of the magnetic properties requires the collection of data to lower temperatures on samples of MnFeMn doped into MnCoMn, and these experiments are currently in progress.

Acknowledgment. This work is partly based on the experiments carried out at the Swiss Light Source, Paul Scherrer Institut, Villigen, Switzerland. The project was supported by the Swiss National Science Foundation, under the auspices of the SCOPES program. We thank Professor Silvio Decurtins for the use of the SQUID magnetometer. We also thank Oksana Zaharko for invaluable assistance with the heat capacity measurements and Paolo Santini for engaging discussions on molecular field theory.

Supporting Information Available: Additional figures. This material is available free of charge via the Internet at http://pubs.acs.org.

IC801727P